ARTICLE **OPEN**

Sea ice loss of the Barents-Kara Sea enhances the winter warming over the Tibetan Plateau

Anmin Duan [1,2,3 ✉], Yuzhuo Peng [1,2], Jiping Liu[4], Yuhang Chen[1,2], Guoxiong Wu[1,2], David M. Holland[5], Bian He[1,2], Wenting Hu[1,2], Yuheng Tang [1,2] and Xichen Li[1,2]

The Tibetan Plateau (TP) is known as one of the most sensitive regions to climate change, and it has experienced accelerated warming in recent decades. However, to what degree the TP warming amplification relates to remote forcing such as sea ice loss in the Arctic sea ice remains unclear. Here, we found that the decline of sea ice concentration over the Barents-Kara Sea (BKS) could account for 18–32% of the winter warming over the TP by comparing observational data and ensemble experiments from an atmospheric general circulation model. The reduced BKS sea ice and resultant upward turbulent heat fluxes can intensify a Rossby wave train propagating equatorward to the TP. As a result, the enhanced southwesterlies towards the TP strengthen the warm advection over most parts of the TP and lead to TP warming. In addition, an atmospheric teleconnection between the Arctic and the TP also exists in the interannual variability. That is, a tripole mode in air temperature, with warm centers in the Arctic and TP but a cold center in the mid-high latitudes of the Eurasian continent in between. Our results imply that the BKS sea ice loss could intensify such a tripole mode and thus enhancing the winter TP warming.

INTRODUCTION

The Tibetan Plateau (TP, often called the third pole) covers an area of about 2.5 million square kilometers with an average altitude of over 4000 m[1]. It holds thousands of glaciers and is the source of many Asian rivers such as the Yellow River and Yangtze River[2,3]. Serving as the water tower of Asia[4,5], the rivers originating from the TP provide water for about 40% of the world's population. The unique topography of the TP exerts a significant influence on the Asian monsoon and even the global climate through the dynamic and thermal effects[6–9]. In the context of global warming, the annual warming rate in the TP is 0.34 °C/decade during 1979–2020 based on the ERA5 reanalysis[10], which is faster than the global average and second only to the Arctic among all regions in the world[10–12]. The observed warming trend exists in all seasons but the strongest warming occurs in winter, followed by autumn[10–12]. As a result, the frequency and intensity of extreme weather and climate events in the TP have increased significantly[13], and the glaciers have melted intensively[3,14]. The reasons behind the enhanced TP warming are complex, and some mechanisms have been proposed, including the increase of greenhouse gas emissions[9,15] and atmospheric water vapor[16,17], snow and ice albedo feedback[17,18], the weakened winter monsoon[19], increased lower clouds[20,21] and brown clouds[22,23], and the land use[24,25]. However, it is not yet clear which process is dominant.

Meanwhile, owing to the unique environmental characteristics and rich natural resources, the Arctic has attracted much attention from scientists and governments worldwide[26–28]. The climate in the Arctic has undergone unprecedented changes. Particularly, the near-surface temperature of the Arctic has risen at a rate more than twice the global average[29] and even more than four times in winter during the recent decades. This phenomenon is known as the Arctic amplification (AA), which has unneglectable regional and global influences[30,31]. The mechanisms responsible for the AA have been widely discussed[32–37], and some studies[36,37] indicate that the Arctic sea ice loss[38,39] plays an important contribution.

So far, however, there have been no reports connecting the TP warming with the rapid change in the Arctic sea ice to our knowledge. It is suggested that the reduction of the Arctic sea ice can intensify aerosol transport to the TP[40], increase the frequency of Indian Summer Monsoon Rainfall extremes[41] and heatwaves in southwestern China[42], and deepen the East Asian Trough in late winter[43]. This study aims to detect the possible contribution of the sea ice loss in the Arctic to the TP winter warming quantitatively by data analysis and numerical experiments from an atmospheric general circulation model (AGCM).

RESULTS

Changes in surface air temperature and Arctic sea ice concentration

As indicated in Fig. 1a, the linear trend of winter surface air temperature (SAT) during 1979–2018 presented by the ERA5 reanalysis can reach above 2 °C/decade in the northeastern BKS. Meanwhile, a significant warming trend also exists in the TP. Along with the dramatic Arctic warming, the sea ice concentration (SIC) in the northeastern BKS has declined rapidly by more than 20% per decade (Fig. 1b). A numerical sensitivity experiment with prescribed observed SIC and surface sea temperature (SST) in the BKS (named as BKS experiment; see details in Methods) demonstrates that the SIC change in BKS could enhance the winter TP warming. Note that the warming magnitude in the Arctic derived from the BKS experiment is similar to the ERA5 (Fig. 1c). Moreover, the decrease of BKS SIC induces a significant cooling trend in the mid-high latitudes of the Eurasia continent

[1]State Key Laboratory of Numerical Modeling for Atmospheric Sciences and Geophysical Fluid Dynamics (LASG), Institute of Atmospheric Physics, Chinese Academy of Sciences, Beijing, China. [2]University of Chinese Academy of Sciences, Beijing, China. [3]State Key Laboratory of Marine Environmental Science, College of Ocean and Earth Sciences, Xiamen University, Xiamen, China. [4]Department of Atmospheric and Environmental Sciences, State University of New York, Albany, NY, USA. [5]Courant Institute of Mathematical Sciences, New York University, New York, NY, USA. ✉email: amduan@lasg.iap.ac.cn
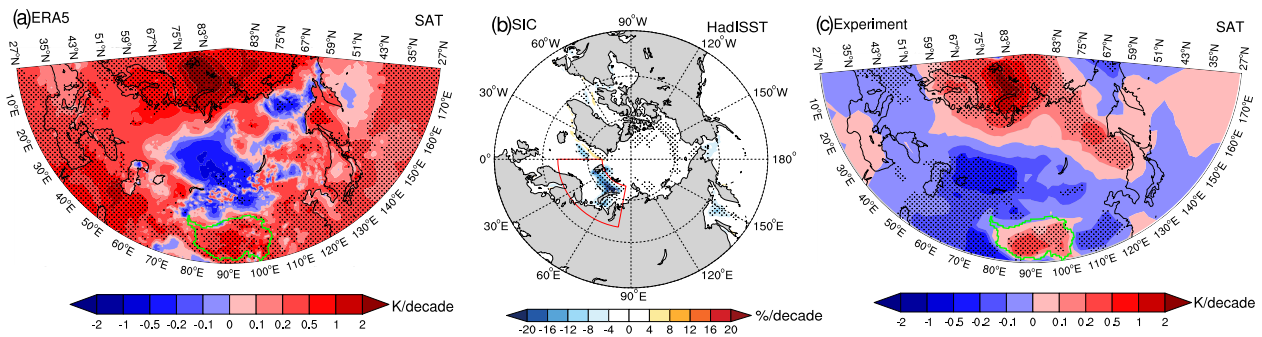
Fig. 1 Linear trends of the winter SAT and SIC during 1979–2018. a Linear trend in the winter SAT derived from ERA5 reanalysis (K/decade); **b** Linear trend in the winter SIC derived from HadISST dataset (%/decade); **c** The same as in **a**, but for BKS experiment results (K/decade). Stippled areas indicate regions exceeding the 90% statistical confidence level. The areas of the Tibetan Plateau (TP) with altitude above 2500 m are shown by green lines in **a** and the region of BKS (65°–80°N, 0°–80°E) is outlined by red lines in **b**.

and obvious warming in the TP (Fig. 1c). The maximum warming rates (above 0.5 °C/decade) are located in the western TP, only slightly smaller than the observed warming.

Two leading modes of SAT over Eurasia

As seen from Fig. 1a and c, the striking warming in the Arctic and TP is accompanied by the cooling in mid-high latitudes of the Eurasia continent, although the cooling areas are much smaller in the observations than the sensitivity experiment simulations. In fact, numerous studies have revealed the mechanisms responsible for the Eurasia continent winter cooling. Some of them[44–47] indicated that the cooling in the Eurasia continent is caused mainly by the loss of Arctic sea ice, whereas others[48,49] argued that the contribution of internal atmospheric variability is dominant. To clarify the atmospheric response driven by the Arctic sea ice reduction and the role of internal atmospheric variability in the TP warming, the EOF analysis of the observed SAT is conducted for winter SAT (27°–90°N, 0°–180°E) in the period of 1979–2018. Results show that the first mode (EOF1) and the second mode (EOF2) of winter SAT account for 29.3% and 20.9% of the total variance, respectively. The first mode is a monopole pattern with consistent warming over the Eurasia continent (Fig. 2a). In addition, the first principal component (PC1) is highly correlated with Arctic Oscillation (AO) index, with a correlation coefficient of 0.77, passing the significance test at the 99% level (Fig. 2c). It implies this uniform warming pattern is closely related to the internal atmospheric variability of AO, which is consistent with Mori et al.[46]. The second mode shows a tripole pattern of warm Arctic, cold Eurasia, and warm TP (named as the AET pattern; Fig. 2b), with a high pattern correlation (0.8, passing the 95% significance level) to the BKS experiment as shown in Fig. 1c. The correlation coefficient between PC2 and SIC anomaly averaged over BKS is as high as −0.79, passing the significant test at the 99% level (Fig. 2d). It implies that the AET pattern, independent of AO, is closely connected with the change of BKS SIC. Moreover, the two leading modes of winter SAT are almost the same in different reanalysis datasets (Supplement Figs. 1 and 2), indicating that the dominant patterns of winter SAT are independent of dataset selection.

## Mechanisms of the TP warming connected to the BKS sea ice loss

The first two EOFs of winter SAT from the ensemble mean of 20 members in the BKS experiment are very similar to the observed patterns (Supplementary Fig. 3a, b.vs. Fig. 2a, b). However, the AET pattern becomes the first mode in model simulations, accounting for ~55% of the total variance, while the AO pattern turns into the second mode. To further investigate the potential impact of the BKS sea ice loss on the TP warming, 10 years of lowest and highest

BKS SIC anomaly in the observation are selected as shown in Supplementary Fig. 3c, named as low-ice (LICE) and high-ice (HICE) years, respectively. Obviously, much more positive phases of the AET pattern appear in LICE years and a reverse situation can be found in HICE years (Supplementary Fig. 3d). In contrast, there is barely a difference in AO phases in LICE and HICE years (Supplementary Fig. 3e). Note that the EOF analysis on each member of BKS experiment indicates that most members can reproduce the AET pattern (Supplementary Fig. 4). Therefore, the AET pattern is an internal mode of atmospheric variability, and the reduction of the BKS sea ice is in favor of the occurrence frequency of the AET positive phase. In order to investigate the mechanisms of the influence of the BKS SIC on the TP warming, we calculated the trends of atmospheric circulation caused by the decrease of BKS SIC in the experiment (Fig. 3a, b). Two anticyclone responses can be seen over the Arctic and TP at both 200 and 500 hPa, accompanied by a cyclone response over Eurasia in between. The anticyclonic circulation over the BKS can be explained by the increased upward turbulent heat fluxes related to the BKS sea ice loss (Supplementary Fig. 5), as mentioned in the previous studies[40,50]. It further enhances the propagation of a wave train from the Arctic via Eurasia and then to the TP, corresponding to the negative vorticity response over the Arctic and TP and a positive vorticity response over the Eurasia continent (Supplementary Fig. 6). As a result, the strengthened south-westerlies and warm advection towards the TP (Supplementary Fig. 7a, b) lead to the TP winter warming. It is worth noting that the circulation response to the BKS sea ice loss in the model simulation resembles the regression wind fields against the AET mode in the ERA5 reanalysis (Fig. 3c, d). This means that the reduction of BKS sea ice, as an external forcing, could induce an atmospheric circulation response resemblance to the AET mode, hence enhancing the TP winter warming.

The above results indicate that the sea ice loss in BKS region could strengthen the TP winter warming. Then, we quantitatively analyze the contribution of the BKS sea ice loss to the TP winter warming through the ratios of warming trends between the BKS experiment and multiple datasets. It is indicated that the BKS SIC loss could contribute ~18–32% of the TP winter warming during the period of 1979–2018 (Fig. 4).

DISCUSSION

Based on the observational data analysis and ensemble experiments from an AGCM, this study for the first time proposes and verifies that the dramatical reduction of BKS SIC is an important factor in the TP winter warming. We find that the second mode of winter SAT over Eurasia (27°–90°N, 0°–180°E) links the BKS SIC and the TP warming. The mode (i.e., the AET mode) is characterized by a tripole pattern with warm centers over the Arctic and the TP, and
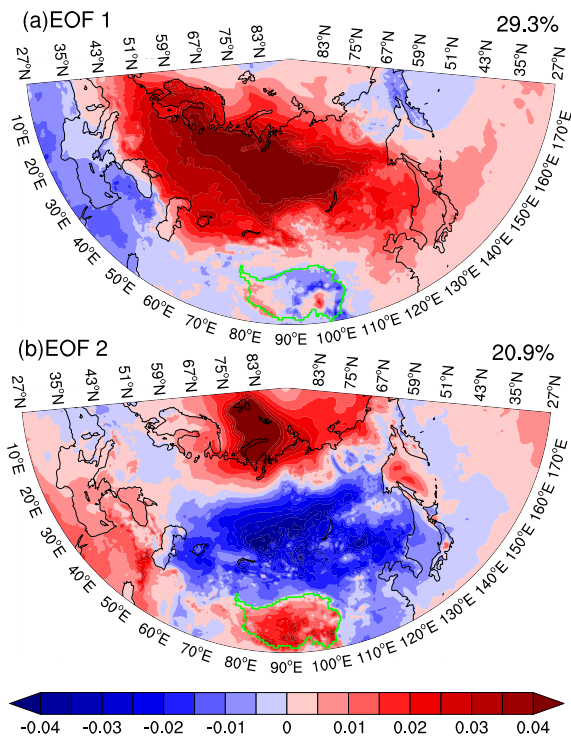
Fig. 2 The two leading modes of winter SAT anomalies (27°–90°N, 0°–180°E). a, b EOF1 and EOF2 of winter mean SAT in ERA5. **c, d** Standardized PC time series (blue lines) and AO index (red line), SIC anomaly (green line, unit: %) in the BKS (axis reversed).

a cold center in the mid and high latitudes of the Eurasian continent. Moreover, the BKS SIC can efficiently regulate the phases of AET, and the reduced BKS sea ice benefits for the occurrence of the AET positive phase. The underlying mechanism could be summarized as that the BKS SIC reduction results in upward turbulent heat fluxes, which promotes the Rossby wave train extension from the Arctic through the Eurasian continent to the TP. Subsequently, the intensified southwesterlies toward the TP reinforce the warm advection and the winter warming over the TP.

This study focuses on the linear trend of winter SAT. Does the physical connection also exist between the BKS SIC and TP SAT anomalies on the interannual time scale? To address this issue, we calculated the correlation between the observed winter BKS SIC anomaly and winter SAT anomaly after removing the linear trend (Supplementary Fig. 8a). It is shown that the less BKS SIC is accompanied by higher SAT over the TP. In addition, the correlation coefficient between the AET and BKS SIC anomaly after removing the linear trend is −0.65, passing the significance test at the 99% significance level. A similar result can also be found in the BKS experiment (Supplementary Fig. 8b–d), despite the anomalies are not significant over the TP and the Eurasia continent. Therefore, the influence of BKS SIC may exist in both variability and trend. Since the decline of BKS SIC can account for 18–32% of the winter warming over the TP, other drivers for the winter SAT anomaly over TP need to be explored further. Moreover, the future loss of Arctic sea ice may exacerbate the TP winter warming suggested by the simulations of a coupled global climate model[51]. Thus, the model capability in simulating the AET pattern might affect the projected warming amplitude over TP, and this issue will be addressed in the future.

Recent studies indicate that internal variability plays an important role in the BKS sea ice loss in spring[52]. Given the similar decreasing sea ice pattern between the spring and winter over the Arctic, whether the winter BKS sea ice loss is a forced response or driven by internal variability needs to be further investigated in our future study.
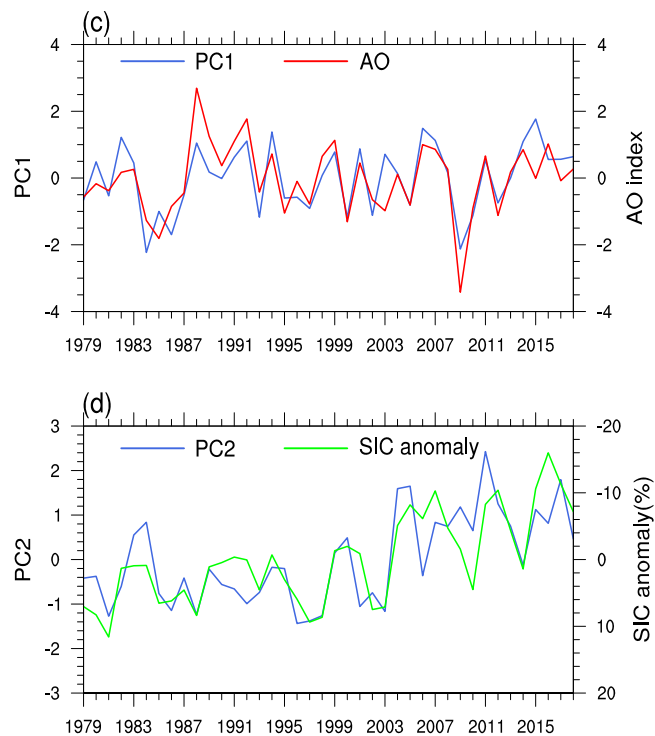
METHODS

We chose the period of 1979–2019 in the above datasets for diagnoses. The winter season includes December in the current year, January and February in the next year. Taking 2018 winter as an example, it is defined as the average value of December 2018 and January–February 2019, and the similar for other years.

Model simulation

The AGCM, i.e., Community Atmosphere Model version 5 (CAM5)[53] with 2.5° × 2.5° horizontal resolution was used to explore whether the observed reduction in the BKS sea ice has an impact on the TP winter warming from 1979 to 2019. We performed an ensemble experiment with 20 members by perturbing the initial condition of each ensemble member.

We first performed a control run lasting for 30 model years. The model states of the beginning (January 1st) of each year from year 11 to year 30 have been used as the initial condition of each ensemble member in the experiments.

We used the same initial condition of the sea ice thickness for each ensemble member, based on the default initial condition of the model, while the sea ice thermal dynamic module is active in this simulation. Each ensemble member starts on January 1st of 1978. After a 1 year spin-up of the atmospheric model and the sea ice thermal dynamic module, the sea ice thickness achieves an equilibrium state. We then start our model experiments for each ensemble member, from Jan 1st of 1979.

In each member, the atmospheric model was driven by the observed monthly sea ice and the sea surface temperature over the BKS (65°–80°N, 0°–80°E) from 1979 to 2019 in the Hadley SST and SIC datasets, whereas the SST and SIC forcings over the other ocean areas were the climatological means with a seasonal cycle. There is a linear buffer zone between the forcing areas and other areas, whose width is 10-degree latitudes (and longitudes). We calculated the ensemble mean of the simulation results of these 20 ensemble members, which is considered to be the response of the model to the observed BKS SIC.

Statistical analysis

The two-tailed Student's t-test was used when the statistical significance was assessed. The least-squares linear trend was removed at each grid point when discussing the interannual variability.
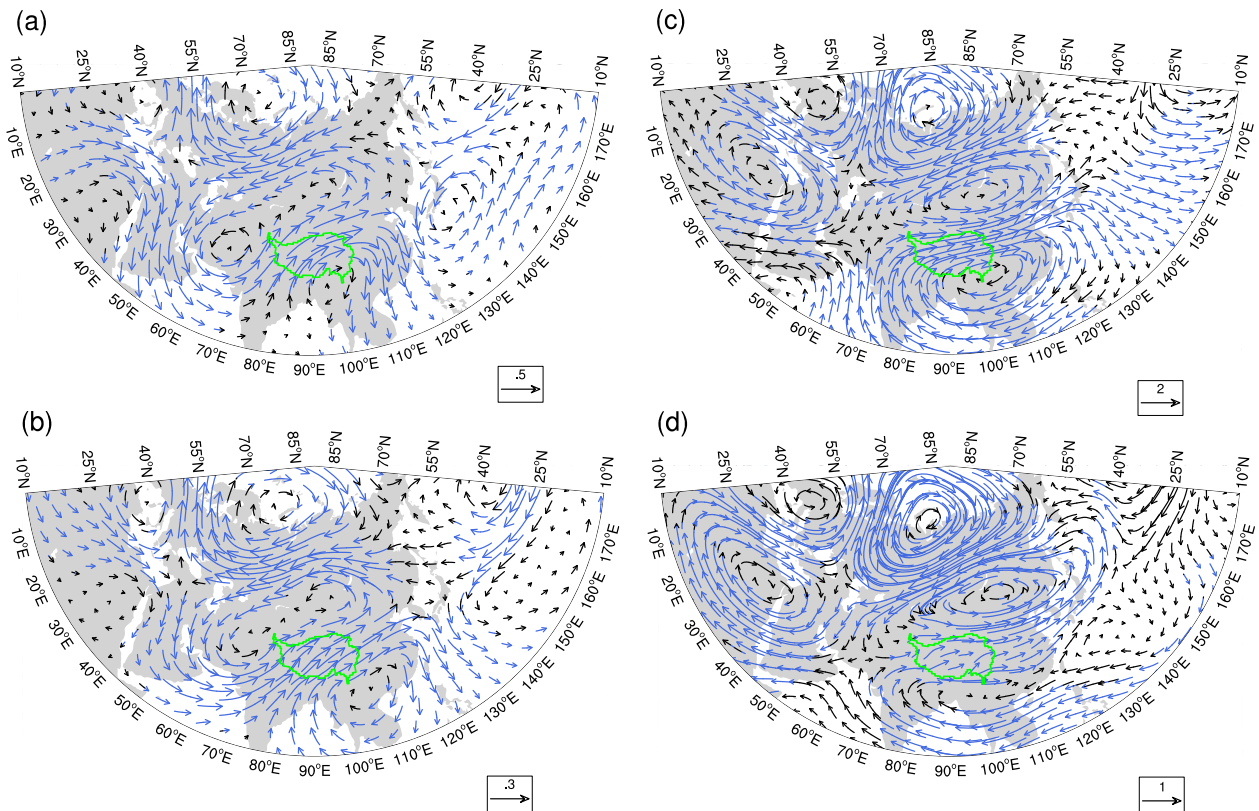
Fig. 3 Observed and simulated wind fields. a, b Linear trends of horizontal wind fields (m s^{-1} decade^{-1}) at 200 hPa (**a**) and 500 hPa (**b**) obtained by the BKS experiment; **c, d** Regressed horizontal wind fields (m s^{-1}) at 200 hPa (**c**) and 500 hPa (**d**) against the normalized PC2 of winter SAT anomalies in the region of Eurasia from 1979 to 2018 derived from ERA5. Blue streamlines indicate the regions exceeding the 90% statistical confidence level. The TP domain is outlined by green curves with the surface altitude above 2500 m.
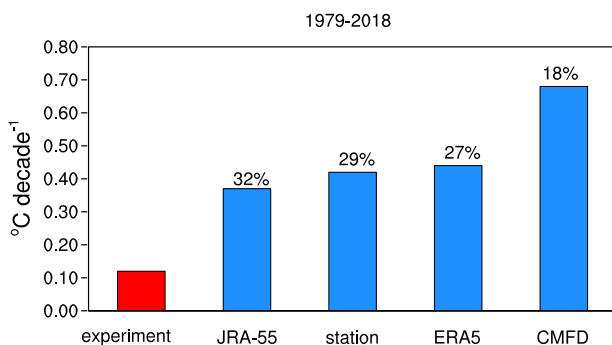
Fig. 4 Contribution of BKS sea ice loss to the TP winter warming. Ratios of warming trends between the BKS experiment and multiple datasets during the period of 1979–2018.

DATA AVAILABILITY

The monthly mean atmospheric variables are from ECMWF-ERA5 on 0.25° × 0.25° spatial resolution[54] (https://www.ecmwf.int/en/forecasts/datasets/reanalysis-datasets/era5). We also use the monthly mean surface air temperature from the JRA55 on the TL319 version with a Gaussian grid (320 latitudes multiplied by 640 longitudes)[55] (http://search.diasjp.net/en/dataset/JRA55), ERA-interim on 1° × 1° spatial resolution[56] (https://www.ecmwf.int/en/forecasts/datasets/reanalysis-datasets/era-interim), NCEP2 on 2.5° × 2.5° spatial resolution[57] (https://www.cpc.ncep.noaa.gov/products/wesley/reanalysis2/). The SAT of 293 stations over the Tibetan Plateau (TP) from the China Meteorological Administration were used for the period 1979–2019. The surface air temperature observational data of the China Meteorological Forcing Dataset (CMFD)[58] on 0.1° × 0.1° spatial resolution used in this study are openly available at http://poles.tpdc.ac.cn/en/data/8028b944-daaa-4511-8769-965612652c49/). The observed sea ice

concentration on 1° × 1° spatial resolution was derived from the HadISST dataset from the UK Met Office[59] (https://www.metoffice.gov.uk/hadobs/hadisst/data/download.html). The AO index was obtained from Climate Prediction Center (https://www.cpc.ncep.noaa.gov/products/precip/CWlink).

CODE AVAILABILITY

All the codes used here are available from the corresponding author on reasonable request.

REFERENCES

1. Qiu, J. China: The third pole. *Nature* **454**, 393–396 (2008).
2. Bolch, T. et al. The state and fate of himalayan glaciers. *Science* **336**, 310–314 (2012).
3. Yao, T. et al. Recent third pole's rapid warming accompanies cryospheric melt and water cycle intensification and interactions between monsoon and environment: multidisciplinary approach with observations, modeling, and analysis. *Bull. Am. Meteorol. Soc.* **100**, 423–444 (2019).
4. Immerzeel, W. W., Van Beek, L. P. H. & Bierkens, M. F. P. Climate change will affect the asian water towers. *Science* **328**, 1382–1385 (2010).
5. Zhao, Y. & Zhou, T. Asian water tower evinced in total column water vapor: a comparison among multiple satellite and reanalysis data sets. *Clim. Dyn.* **54**, 231–245 (2020).
6. Duan, A., Hu, D., Hu, W. & Zhang, P. Precursor effect of the Tibetan Plateau heating anomaly on the seasonal March of the East Asian Summer Monsoon precipitation. *J. Geophys. Res. Atmos.* **125**, 1–20 (2020).
7. Sun, R. et al. Interannual variability of the north Pacific mixed layer associated with the spring tibetan plateau thermal forcing. *J. Clim.* **32**, 3109–3130 (2019).

8. Liu, Y. et al. Land-atmosphere-ocean coupling associated with the Tibetan Plateau and its climate impacts. *Natl Sci. Rev.* **7**, 534–552 (2020).

9. Duan, A., Wu, G., Liu, Y., Ma, Y. & Zhao, P. Weather and climate effects of the Tibetan Plateau. *Adv. Atmos. Sci.* **29**, 978–992 (2012).

10. You, Q. et al. Warming amplification over the Arctic Pole and Third Pole: trends, mechanisms and consequences. *Earth Sci. Rev.* **217**, 103625 (2021).

11. Ma, J. et al. The dominant role of snow/ice Albedo feedback strengthened by black carbon in the enhanced warming over the Himalayas. *J. Clim.* **32**, 5883–5899 (2019).

12. Duan, A. & Xiao, Z. Does the climate warming hiatus exist over the Tibetan Plateau? *Sci. Rep.* **5**, 13711 (2015).

13. You, Q., Kang, S., Aguilar, E. & Yan, Y. Changes in daily climate extremes in the eastern and central Tibetan Plateau during 1961–2005. *J. Geophys. Res. Atmos.* **113**, 1–17 (2008).

14. Yao, T. et al. Different glacier status with atmospheric circulations in Tibetan Plateau and surroundings. *Nat. Clim. Chang.* **2**, 663–667 (2012).

15. Guo, D. & Wang, H. The significant climate warming in the northern Tibetan Plateau and its possible causes. *Int. J. Climatol.* **32**, 1775–1781 (2012).

16. Rangwala, I., Miller, J. R., Russell, G. L. & Xu, M. Using a global climate model to evaluate the influences of water vapor, snow cover and atmospheric aerosol on warming in the Tibetan Plateau during the twenty-first century. *Clim. Dyn.* **34**, 859–872 (2010).

17. Gao, K., Duan, A., Chen, D. & Wu, G. Surface energy budget diagnosis reveals possible mechanism for the different warming rate among Earth's three poles in recent decades. *Sci. Bull.* **64**, 1140–1143 (2019).

18. You, Q., Min, J. & Kang, S. Rapid warming in the tibetan plateau from observations and CMIP5 models in recent decades. *Int. J. Climatol.* **36**, 2660–2670 (2016).

19. You, Q. et al. Climate warming and associated changes in atmospheric circulation in the eastern and central Tibetan Plateau from a homogenized dataset. *Glob. Planet. Change* **72**, 11–24 (2010).

20. Zhang, X., Peng, L., Zheng, D. & Tao, J. Cloudiness variations over the Qinghai-Tibet Plateau during 1971-2004. *J. Geogr. Sci.* **18**, 142–154 (2008).

21. Duan, A. & Wu, G. Change of cloud amount and the climate warming on the Tibetan Plateau. *Geophys. Res. Lett.* **33**, L22704 (2006).

22. You, Q. et al. From brightening to dimming in sunshine duration over the eastern and central Tibetan Plateau (1961–2005). *Theor. Appl. Climatol.* **101**, 445–457 (2010).

23. Ramanathan, V. et al. Warming trends in Asia amplified by brown cloud solar absorption. *Nature* **448**, 575–578 (2007).

24. Cui, X. & Graf, H. F. Recent land cover changes on the Tibetan Plateau: a review. *Clim. Change* **94**, 47–61 (2009).

25. You, Q., Fraedrich, K., Ren, G., Pepin, N. & Kang, S. Variability of temperature in the Tibetan Plateau based on homogenized surface stations and reanalysis data. *Int. J. Climatol.* **33**, 1337–1347 (2013).

26. Landrum, L. & Holland, M. M. Extremes become routine in an emerging new Arctic. *Nat. Clim. Chang.* **10**, 1108–1115 (2020).

27. Terhaar, J., Kwiatkowski, L. & Bopp, L. Emergent constraint on Arctic Ocean acidification in the twenty-first century. *Nature* **582**, 379–383 (2020).

28. Ouyang, Z. et al. Sea-ice loss amplifies summertime decadal CO2 increase in the western Arctic Ocean. *Nat. Clim. Chang.* **10**, 678–684 (2020).

29. Stocker, T. F. et al. *Climate change 2013 the physical science basis: Working Group I contribution to the fifth assessment report of the intergovernmental panel on climate change. Climate Change 2013 the Physical Science Basis: Working Group I Contribution to the Fifth Assessment Report of the Intergovernmental Panel on Climate Change.* https://doi.org/10.1017/CBO9781107415324 (2013).

30. Bintanja, R. & Van Der Linden, E. C. The changing seasonal climate in the Arctic. *Sci. Rep.* **3**, 1–8 (2013).

31. Cohen, J. et al. Recent Arctic amplification and extreme mid-latitude weather. *Nat. Geosci.* **7**, 627–637 (2014).

32. Feldl, N., Po-Chedley, S., Singh, H. K. A., Hay, S. & Kushner, P. J. Sea ice and atmospheric circulation shape the high-latitude lapse rate feedback. *npj Clim. Atmos. Sci.* **3**, 1–9 (2020).

33. Stuecker, M. F. et al. Polar amplification dominated by local forcing and feedbacks. *Nat. Clim. Chang.* **8**, 1076–1081 (2018).

34. Pithan, F. & Mauritsen, T. Arctic amplification dominated by temperature feedbacks in contemporary climate models. *Nat. Geosci.* **7**, 181–184 (2014).

35. Winton, M. Amplified Arctic climate change: what does surface albedo feedback have to do with it? *Geophys. Res. Lett.* **33**, 279–296 (2006).

36. Screen, J. A. & Simmonds, I. The central role of diminishing sea ice in recent Arctic temperature amplification. *Nature* **464**, 1334–1337 (2010).

37. Dai, A., Luo, D., Song, M. & Liu, J. Arctic amplification is caused by sea-ice loss under increasing CO2. *Nat. Commun.* **10**, 1–13 (2019).

38. Stroeve, J. C. et al. Trends in Arctic sea ice extent from CMIP5, CMIP3 and observations. *Geophys. Res. Lett.* **39**, 1–7 (2012).

39. Comiso, J. C., Meier, W. N. & Gersten, R. Variability and trends in the Arctic Sea ice cover: results from different techniques. *J. Geophys. Res. Ocean.* **122**, 6883–6900 (2017).

40. Li, F. et al. Arctic sea-ice loss intensifies aerosol transport to the Tibetan Plateau. *Nat. Clim. Chang.* **10**, 1037–1044 (2020).

41. Chatterjee, S., Ravichandran, M., Murukesh, N., Raj, R. P. & Johannessen, O. M. A possible relation between Arctic sea ice and late season Indian Summer Monsoon Rainfall extremes. *npj Clim. Atmos. Sci.* **4**, 1–6 (2021).

42. Deng, K., Jiang, X., Hu, C. & Chen, D. More frequent summer heat waves in southwestern China linked to the recent declining of Arctic sea ice. *Environ. Res. Lett.* **15**, 074011 (2020).

43. Xu, M., Tian, W., Zhang, J., Wang, T. & Qie, K. Impact of sea ice reduction in the barents and kara seas on the variation of the East Asian trough in late winter. *J. Clim.* **34**, 1081–1097 (2021).

44. Zhang, P., Wu, Y., Chen, G. & Yu, Y. North American cold events following sudden stratospheric warming in the presence of low Barents-Kara Sea sea ice. *Environ. Res. Lett.* **15**, 124017 (2020).

45. De, B. & Wu, Y. Robustness of the stratospheric pathway in linking the Barents-Kara Sea ice variability to the mid-latitude circulation in CMIP5 models. *Clim. Dyn.* **53**, 193–207 (2019).

46. Mori, M., Watanabe, M., Shiogama, H., Inoue, J. & Kimoto, M. Robust Arctic sea-ice influence on the frequent Eurasian cold winters in past decades. *Nat. Geosci.* **7**, 869–873 (2014).

47. Mori, M., Kosaka, Y., Watanabe, M., Nakamura, H. & Kimoto, M. A reconciled estimate of the influence of Arctic sea-ice loss on recent Eurasian cooling. *Nat. Clim. Chang.* **9**, 123–129 (2019).

48. McCusker, K. E., Fyfe, J. C. & Sigmond, M. Twenty-five winters of unexpected Eurasian cooling unlikely due to Arctic sea-ice loss. *Nat. Geosci.* **9**, 838–842 (2016).

49. Ogawa, F. et al. Evaluating impacts of recent Arctic sea ice loss on the Northern hemisphere winter climate change. *Geophys. Res. Lett.* **45**, 3255–3263 (2018).

50. Honda, M., Inoue, J. & Yamane, S. Influence of low Arctic sea-ice minima on anomalously cold Eurasian winters. *Geophys. Res. Lett.* **36**, L08707 (2009).

51. Sun, L., Alexander, M. & Deser, C. Evolution of the global coupled climate response to Arctic sea ice loss during 1990–2090 and its contribution to climate change. *J. Clim.* **31**, 7823–7843 (2018).

52. England, M., Jahn, A. & Polvani, L. Nonuniform contribution of internal variability to recent Arctic sea ice loss. *J. Clim.* **32**, 4039–4053 (2019).

53. Neale, R. B. et al. Description of the NCAR Community Atmosphere Model (CAM 5.0). *NCAR Tech. Notes* **1**, 1–14 (2012).

54. Hersbach, H. et al. The ERA5 global reanalysis. *Q. J. R. Meteorol. Soc.* **146**, 1999–2049 (2020).

55. Kobayashi, S. et al. The JRA-55 reanalysis: General specifications and basic characteristics. *J. Meteorol. Soc. Jpn.* **93**, 5–48 (2015).

56. Dee, D. P. et al. The ERA-Interim reanalysis: configuration and performance of the data assimilation system. *Q. J. R. Meteorol. Soc.* **137**, 553–597 (2011).

57. Kanamitsu, M. et al. NCEP-DOE AMIP-II reanalysis (R-2). *Bull. Am. Meteorol. Soc.* **83**, 1631–1644 (2002).

58. He, J. et al. The first high-resolution meteorological forcing dataset for land process studies over China. *Sci. Data* **7**, 1–11 (2020).

59. Rayner, N. A. et al. Global analyses of sea surface temperature, sea ice, and night marine air temperature since the late nineteenth century. *J. Geophys. Res. Atmos.* **108**, 4407 (2003).

AUTHOR CONTRIBUTIONS

A.M.D. designed the structure of the paper and revised the paper. Y.Z.P. wrote the initial paper and carried out most of the data analysis. Y.H.C. and Y.H.T. helped in the analysis of the data. X.C.L. conducted the numerical experiments. G.X.W., D.M.H., B.H., J.P.L., and W.T.H. checked the paper and proposed amendments. All authors contributed to the paper and approved the submitted version.

COMPETING INTERESTS

The authors declare no competing interests.

ADDITIONAL INFORMATION